Structures of elemental potassium at terapascal pressures

Jack Whaley-Baldwin [*]

TCM Group, Cavendish Laboratory, University of Cambridge, J. J. Thomson Avenue,
Cambridge CB3 0HE, United Kingdom

We investigate the pressure-temperature phase diagram of elemental potassium (K) up to multiterapascal (TPa) pressures using *ab initio* random structure searching (AIRSS), discovering eight structural phase transitions beyond the already known double hexagonal close-packed (dhcp) structure. Starting at 1.15 TPa, K transitions from the dhcp structure and passes through a variety of close-packed hexagonal and trigonal phases (dhcp $\rightarrow$ $P6_3/mmc \rightarrow P3m1 \rightarrow P\bar{6}m2$), which differ only in their stacking sequence along the c axis. At 2.55 TPa, K adopts the hexagonal close-packed (hcp) structure, and at 7.21 TPa transitions into a complex orthorhombic phase of $Fddd$ symmetry with 64 atoms in its (conventional) unit cell, before assuming an $Ibam$ structure at 8.60 TPa, and, eventually, the face centered cubic (fcc) structure at 23.6 TPa, which persists well into the petapascal (PPa) regime. Further, we calculate the full pressure-temperature dependence of the melting line of K through extensive molecular dynamics simulations. We study the evolution of the bonding topology of K with pressure, finding that K passes through two *quasi*-molecular phases featuring diatomic pairs (the $Fddd$ and $Ibam$ structures), before ultimately becoming a high pressure electride (HPE) in the fcc phase. The electron-phonon and superconducting properties of K at these extreme pressures are also investigated, where we find the critical temperature T_c rises to a maximum of between 7.65 K and 15.70 K in the hcp phase, before eventually decreasing to essentially zero in the fcc phase. Our results fully elucidate the structural and electronic behavior of K under the most extreme conditions, and provide new case studies for multi-TPa dynamic compression experiments.

I. INTRODUCTION

Under ambient conditions, the group-I alkali metals form simple crystalline phases with electronic structures that are well described by the nearly-free electron (NFE) approximation. This simplistic picture changes in every possible way upon application of pressure; they form structurally complex incommensurate host-guest (HG) phases [1,2], become wide-gap insulators [3,4], and their optical properties change to such an extent that they become transparent in the visible spectrum [3–5].

Potassium (K) is a particularly striking example of the structural and electronic complexity encountered in the alkali metals under compression. K assumes a body-centered cubic (bcc) structure at ambient pressure, transitioning to face-centered cubic (fcc) at 11.6 GPa [6]. With further increases in pressure, K transforms into an incommensurate HG structure [2], the orthorhombic (*Pnma*) oP8 structure [7], tetragonal (*I4₁/amd*) tI4 structure [7], orthorhombic (*Cmca*) oC16 structure [7] and, finally, the double hexagonal close-packed (dhcp) structure above 250 GPa [8]. Throughout this remarkable transition sequence, K goes from being a good conductor in the ambient bcc phase to an insulating electride in the oP8 structure, before reverting back to metallic behavior in the dhcp phase.

Over the past decade, advances in dynamic compression techniques have succeeded in achieving experimental pressures of up to 5 TPa [9–21], with developments in powder diffraction methods allowing the crystal structures of such dense matter to be glimpsed [22–24]. Of particular interest in these experiments is the behavior of the elements under pressure, since they provide a relatively clean (that is; free of complications due to changes in stoichiometry) testing ground for cutting-edge compression techniques [9–16], and are useful as ultrahigh-pressure reference materials [11,12]. As such, *ab initio* determination of the equations of state for the elements under such conditions is of profound importance. Such extreme environments also provide for a robust comparison between theory (DFT) and experiment.

Since the behavior of K is so rich under even moderate compression, it is of interest to see whether this structural and electronic complexity continues into the terapascal regime. Whilst the lighter group-I element sodium (Na) has been studied using *ab initio* methods up to pressures of 20 TPa [25], no such investigation has been carried out on K. The study of matter at such extreme pressures has given rise to an enormous array of noteworthy phenomena, such as the metallization of helium [26], the decomposition of water ice [27], and the total suppression of superconductivity in sulfur [28].

In this paper, we perform a detailed computational structure search to completely reveal the solid-state phase diagram of elemental K under extreme pressure-temperature conditions, and extend our results to the liquid state by calculating the melting line as a function of (p, T). We uncover a
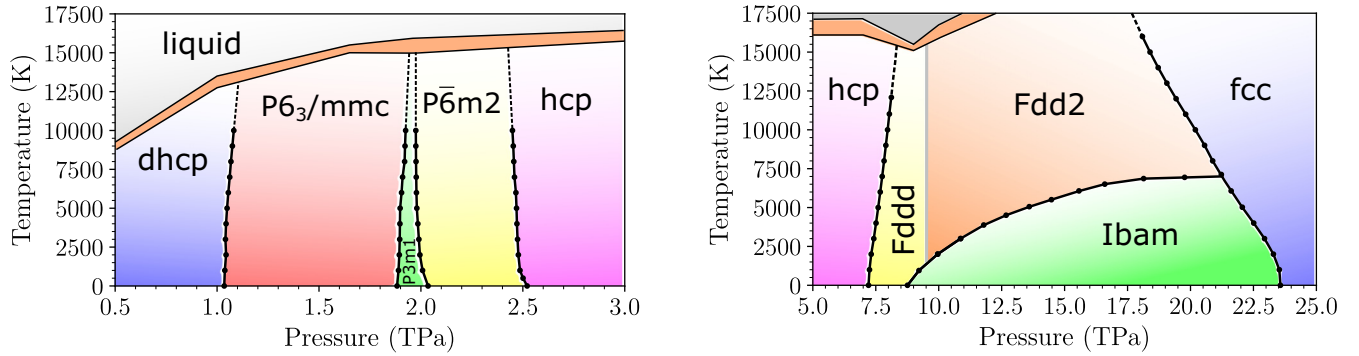
---

[*]jajw4@cam.ac.uk

024106-1

FIG. 1. Phase diagrams up to 25 TPa. Each coloured region denotes the structure with the lowest Gibbs free energy, with $G(T, p) = U_{\text{elec}} + U_{\text{phonon}} - TS_{\text{elec}} - TS_{\text{phonon}} + pV$. In the solid state, vibrational effects are included at the level of the harmonic approximation (HA), and solid circles on the phase boundaries denote explicitly calculated (T, p) points according to the HA. The melting line, as calculated using molecular dynamics simulations (see text), is shown as a thick-orange line. The dashed lines between the solid-state phase boundaries and the melting line indicate regions where the solid is anharmonic. The solid-grey vertical line at ~ 9.50 TPa on the right plot marks a second-order phase boundary between the $Fddd$ and $Fdd2$ structures.

remarkable phase transition sequence, and observe an unusual charge density distribution, which seems to suggest that K forms molecular-like bonds under sufficient compression, whilst still managing to remain metallic.

II. COMPUTATIONAL DETAILS

The *ab initio* random structure searching (AIRSS) package [29,30] was used to perform our structure search, with the first-principles density functional theory (DFT) code CASTEP [31] performing the underlying electronic structure calculations. We performed structure searches at 1, 2.5, 5, 7.5, 10, 25, 50, and 100 TPa, using randomly constructed unit cells containing between 1 and 30 atoms, and possessing between 1 and 48 symmetry operations. Each search produced approximately 2000 relaxed structures, giving around 16 000 structures in total. As will be discussed in detail later, an extra dataset of 3556 structures at 1.90 TPa comprising only differently-stacked hexagonal and trigonal structures was constructed, in order to more densely sample this particular region of the potential energy surface (PES). For both the structure searches and our final results presented here, we constructed a special ultrasoft pseudopotential that explicitly included core (n = 2) and valence (n = 3, n = 4) electrons (requiring a plane-wave cutoff of 2 keV), and for our paper above 75 TPa, we constructed an all-electron ultrasoft pseudopotential (requiring a plane-wave cutoff of 28 keV). Due to small enthalpy differences between certain competing phases, we used a dense **k**-point sampling of $2\pi \times 0.015$ Å^{-1}. We found that these parameters were sufficient for absolute convergence of total energies to better than 0.5 meV, with relative convergence being even better than this. Full details of our calculations can be found in the Supplemental Material [32].

III. RESULTS AND DISCUSSION

Figure 1 presents the structures discovered in our search, and shows the high-pressure phase diagram of K extended to finite temperatures just beyond the melting point of K, as calculated using the Perdew-Burke-Ernzerhof (PBE)

exchange-correlation functional [33]. Free energies were calculated using the harmonic approximation (HA) in the solid state, and the melting line was evaluated using a Behler-Parrinello neural-network machine-learned potential (MLP) [34] trained on *ab inito* data using the n2p2 package [35] (see Supplemental Material [32] for details of finite-temperature calculations and MLP training). We note that there is a small region between the solid harmonic regime and the melt state where the solid is necessarily anharmonic (see Fig. 1); we have made no attempt to perform any anharmonic calculations here, instead simply opting to connect these regions. Figure 2 shows the static-lattice enthalpies of the structures as a function of pressure, and static-lattice transition pressures according to the LDA, PBE and PBEsol exchange-correlation functionals can be found in Table I. At zero temperature, we find that the dhcp phase of K is the lowest enthalpy structure until around 1.15 TPa, at which point a large number of hexagonal and trigonal structures start to become lower in enthalpy. These "hexagonally stacked" structures are all similar, and comprise hexagonal layers of atoms stacked in either an A, B, or C arrangement along the hexagonal c-axis, such as ABCAB or ABACBC (for reference, the familiar fcc structure can be represented as ABC, the dhcp structure as ABAC, and the hcp structure as AB). Examples of such structures

TABLE I. Static-lattice transition pressures (in TPa) for the structural phase transitions discussed in this paper, using the PBE, LDA, and PBEsol exchange-correlation functionals. We note that inclusion of vibrational effects (as in Fig. 1) shifts the transition pressures slightly.

Transition	PBE	LDA	PBEsol
dhcp $\to$ $P6_3/mmc$	1.15	1.37	1.26
$P6_3/mmc$ $\to$ $P3m1$	1.85	1.71	1.93
$P3m1 \to P\bar{6}m2$	2.05	2.01	2.11
$P\bar{6}m2 \to$ hcp	2.55	2.50	2.64
hcp $\to Fddd$	7.35	7.29	7.47
$Fddd \to Ibam$	7.94	7.70	7.85
$Ibam \to$ fcc	22.8	22.5	23.1
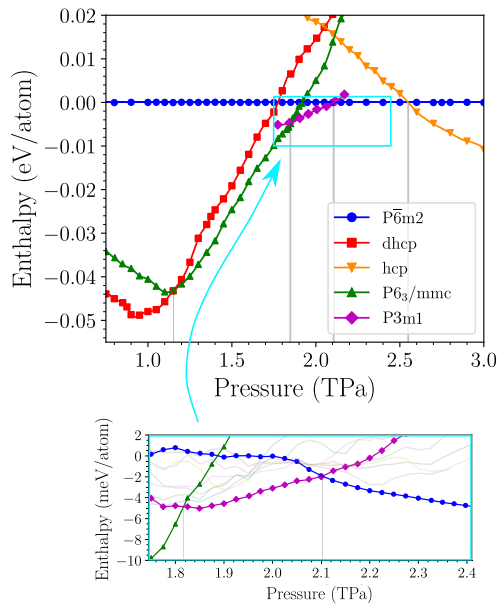
(a)
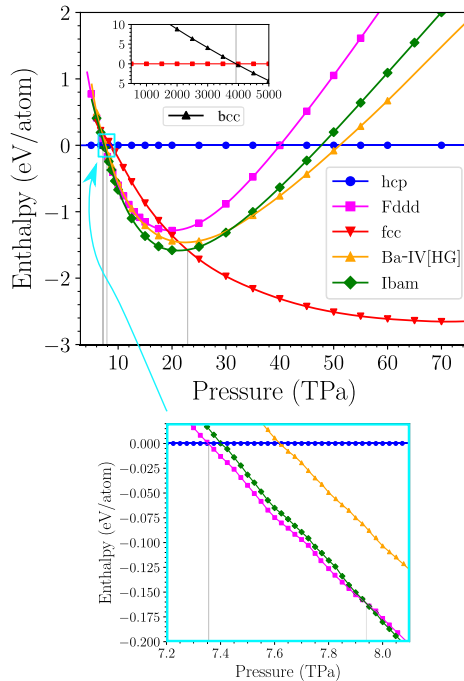
(b)

FIG. 2. Static lattice enthalpies of the structures. Grey-vertical lines mark the phase transitions. (a) Static lattice enthalpies, $0.75 - 3.00$ TPa. The cyan box details the region $1.70 - 2.40$ TPa, and the unmarked faded lines are other, competitive hexagonal stacking sequences (see Fig. 3). (b) Static lattice enthalpies, $3 - 75$ TPa. The cyan box details the region $7.2 - 8.1$ TPa.
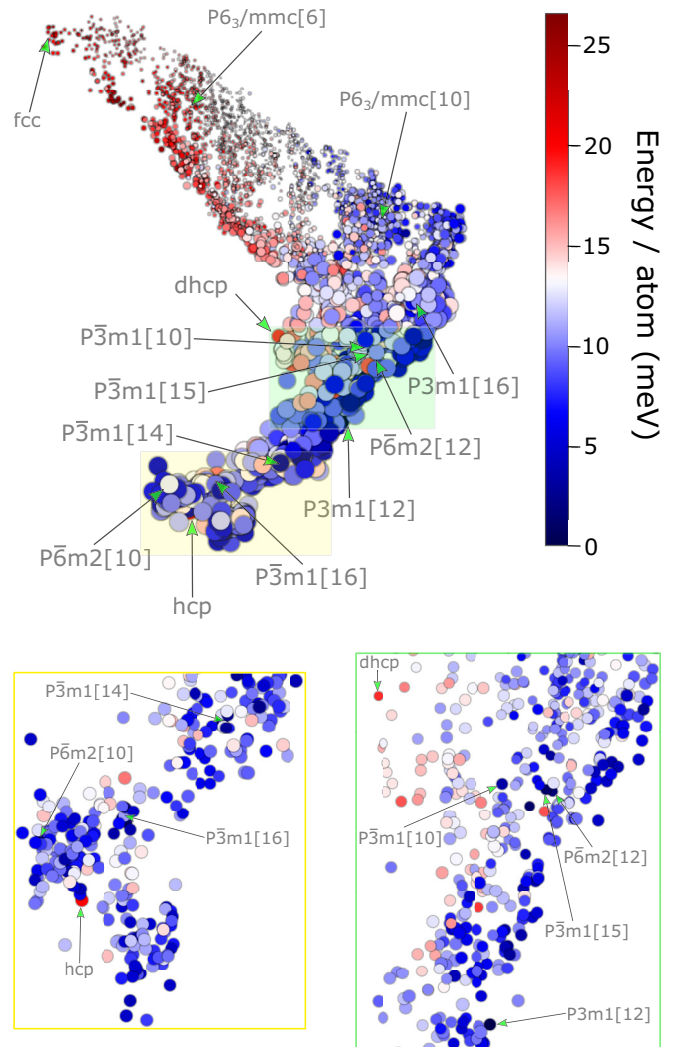

FIG. 3. Three-component UMAP [36] projection of the low-enthalpy hexagonal/trigonal manifold in structure space at 1.90 TPa, from a dataset of 3556 hexagonally stacked structures (see text). The first two UMAP components are plotted horizontally and vertically, and the projection onto the third component is represented by the size of each circle. Particularly low-energy or otherwise interesting structures have been labeled, with the number of atoms in the primitive cell indicated in square brackets.

included an 11-atom $P\bar{3}m1$ structure, 14-atom $P3m1$, 8-atom $P6_3/mmc$, 16-atom $P\bar{6}m2$, 11-atom $R3m$, and a 9-atom $R\bar{3}m$ structure. Given the frequent appearance of these hexagonally stacked structures in our searches, we sought to determine the ideal stacking sequence by sampling this region of structure space particularly densely. We constructed "by hand" all

unique stacking sequences up to 20 layers long (as measured along the c axis) and relaxed them; full details can be found in the Supplemental Material [32]. These different stacking sequences form a nearly-degenerate manifold in structure space, with structures separated by meV energies or less. The situation is illustrated in Fig. 3, which shows the resulting dataset of 3556 structures projected onto a lower-dimensional representation of structure space at 1.90 TPa using the UMAP algorithm [36]. It can be seen that, within this "hexagonally stacked manifold", there exists a subregion slightly lower in energy (the blue circles in Fig. 3), where most of the ideal stacking sequences lie. Of all the structures investigated (both from our original search and those constructed by hand), we found that a sequence 6 layers long, of $P6_3/mmc$ symmetry

and containing six atoms in the primitive cell was the most stable structure in the range 1.15 – 1.84 TPa. Additionally, a sequence 12 layers long, of $P3m1$ symmetry and containing 12 atoms in the primitive cell was the most stable in the range 1.82 – 2.10 TPa, and a sequence 10 layers long, of $P\bar{6}m2$ symmetry and containing 10 atoms in the primitive cell was the most stable in the range 2.10 – 2.55 TPa (whereafter the simple hcp structure becomes the ground state). In some parts of the phase diagram between 1.8 TPa and 2.2 TPa, we find that some other hexagonal/trigonal stacking motifs come within just a few tenths of an meV per atom of being the lowest enthalpy structure. These many competing structures are shown as faint lines on the bottom plot of Fig. 2(a). Even with our extremely strict calculation tolerances therefore, it is not possible to rule out some of these structures from potentially becoming the ground state in some small pressure interval. Owing to this near degeneracy, it is possible that K may in fact adopt a mixture of these differently-stacked structures, or that K would "choose" one particular sequence from this essentially degenerate selection, depending on the history of the sample. It is also possible that the structures in this region represent intermediate, local minima on a pathway in structure space between the dhcp, $P6_3/mmc$, $P3m1$, $P\bar{6}m2$, and hcp phases, as there is no trivial transformation that connects these structures—transitioning from one to the other requires the simultaneous shifting of multiple layers. Such a coexistence situation has been proposed in high-pressure beryllium [37], where a multitude of differently-stacked structures—all of which are metastable—connect a hcp structure to a $R\bar{3}m$ phase.

The $P6_3/mmc$, $P\bar{6}m2$, and $P3m1$ structures are shown in Figs. 4(c), 4(d), and 4(e), respectively, alongside the simpler hcp [Fig. 4(a)] and dhcp [Fig. 4(b)] motifs. Whilst it is possible to describe all of the hexagonally stacked structures in terms of their stacking sequences, a more visually intuitive view is presented in Fig. 4. Every sequence of three layers defines the vertices of a polyhedron (a triangular orthobicupola), and the overall structure can be represented as a particular stacking of these polyhedra, each of which share an edge with another.

At 2.55 TPa, K adopts the simple hcp structure, eventually becoming face-centered cubic (fcc) above 23.6 TPa. Remarkably however, between the simplistic hcp and fcc structures, we predict two further transitions to two complex, non-close-packed phases of $Fddd$ and $Ibam$ symmetry at 7.21 TPa and 8.76 TPa, respectively.

The $Fddd$ structure [shown in Fig. 5(b)] features 64 (16) atoms in its conventional (primitive) unit cell, with K atoms occupying two distinct 32h sites of the conventional orthorhombic cell. Remarkably, this same structure is also realised as a high-pressure phase of elemental sulfur (S) [38]. Above ~9.5 TPa, an imaginary Γ-point phonon appears in the vibrational spectrum of the $Fddd$ structure, which distorts it into a structure of $Fdd2$ symmetry (with the same number of atoms per cell); by this pressure however, a transition to the $Ibam$ structure has already occurred at zero temperature. Nonetheless, this $Fdd2$ phase can be realized at finite temperatures ($\gtrsim$1750 K) owing to its favourable vibrational free energy over the $Ibam$ structure (see Fig. 1). This $Fdd2$ structure meets the phase boundaries of the $Ibam$ and fcc structures

(a) hcp

(b) dhcp

(c) $P6_3/mmc$
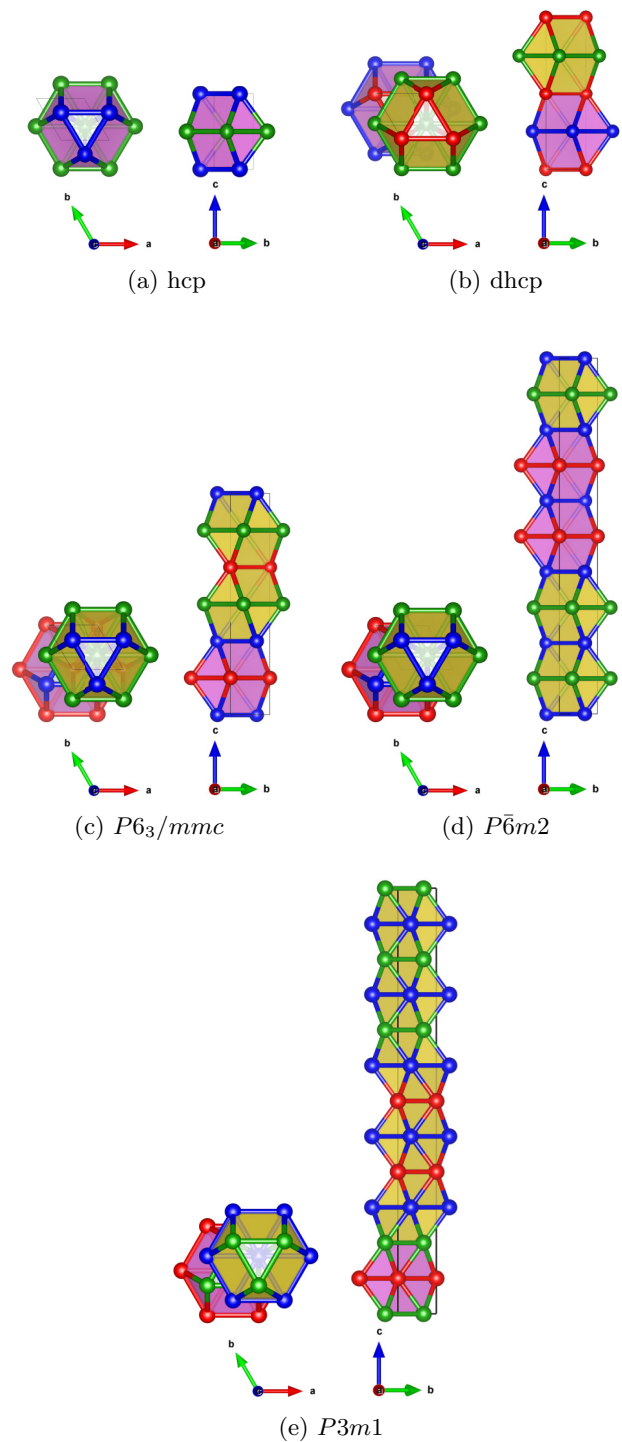
(d) $P\bar{6}m2$

(e) $P3m1$

FIG. 4. The hexagonally-stacked hcp, dhcp, 6-atom $P6_3/mmc$, 10-atom $P\bar{6}m2$, and 12-atom $P3m1$ structures, arranged in order of increasing stacking sequence length. Atoms with a, b coordinates of (0,0), (0.333,0.666), and (0.666,0.333) have been coloured red, green, and blue respectively. Bounding polyhedra are shown in yellow and purple.

at ~7000 K and ~21.2 TPa, resulting in a solid-state triple-point. We also note here a minor peculiarity of the $Fddd$ structure; the melting line of K exhibits a small, but noticeable "dip" in the $Fddd$ phase, compared to the neighboring
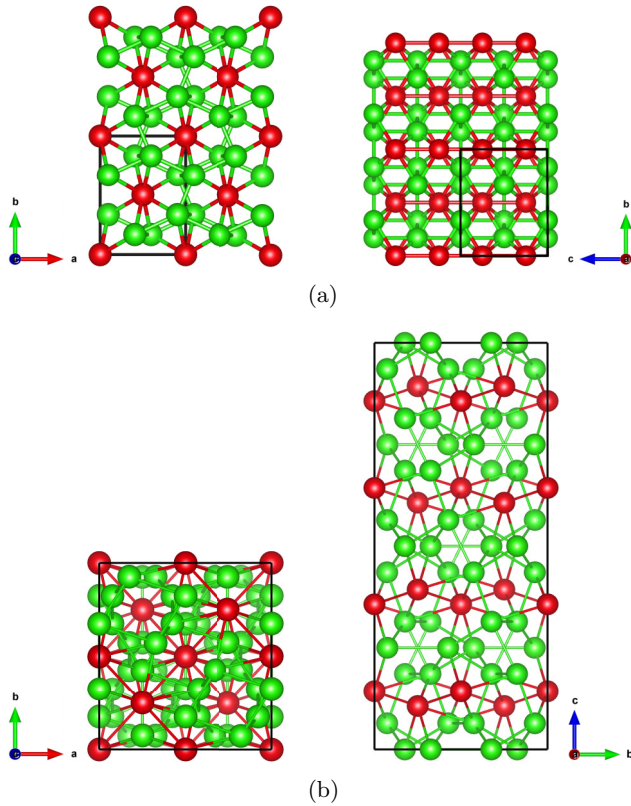
FIG. 5. Structural models of the orthorhombic *Ibam* and *Fddd* structures. The models have been colored in such a way as to highlight the resemblance to the Ba-IV type host-guest structure. (a) *Ibam* structure (shown as a 2 × 2 × 2 supercell), with 8*j* atoms in green and 4a atoms in red. (b) *Fddd* structure, with the two different 32*h* site atoms in green and red.

FIG. 6. Phonon dispersion relations for the structures discussed in this paper, at selected pressures. All phonon calculations were performed on an 8 × 8 × 8 **q**-point grid. (a) dhcp at 1.00 TPa. (b) $P6_3/mmc$ at 1.65 TPa. (c) $P3m1$ at 1.95 TPa. (d) $P\bar{6}m2$ at 2.30 TPa. (e) hcp at 5.00 TPa. (f) *Fddd* at 7.50 TPa. (g) *Ibam* at 9.00 TPa. (h) fcc at 25.0 TPa.

hcp and *Fdd*2 structures (see Fig. 1). The *Ibam* structure [shown in Fig. 5(a)], which K adopts after the $Fddd \rightarrow Ibam$ transition at 8.76 TPa, features 12 (6) atoms in its conventional (primitive) unit cell, with K atoms occupying the 8*j* and 4a sites of the conventional orthorhombic cell. The same structure is realized in the (ambient pressure) phases of SiS_2 and $SiSe_2$ [39], and a computational study has suggested it as a possible metastable phase for high-pressure silicon [40]. As far as we are aware however, K represents the first elemental system for which this *Ibam* structure is the ground state.

Both the *Fddd* and *Ibam* phases bear a striking resemblance to the Ba-IV type "host-guest" (HG) structures found in several elements across the periodic table [2,38,41–45], in that they clearly comprise a "host" framework within which chains of "guest" atoms lie. In fact, a previous publication has shown that the *Fddd* structure is simply a distortion of the Ba-IV HG structure [38]. Interestingly, we find that over the range the *Fddd* and *Ibam* structures are stable, a Ba-IV type host-guest approximant is only ∼50 meV higher in enthalpy [see Fig. 2(b)], although it never quite becomes the lowest enthalpy structure. It should be noted that, at much lower pressures (∼20 GPa), K does indeed possess a (different) HG structure—the K-IIIa and K-IIIb phases [2]. We tried relaxing the K-IIIa and K-IIIb structures at 7.5 TPa, but both collapsed to a simple cubic (SC) structure, indicating that they are
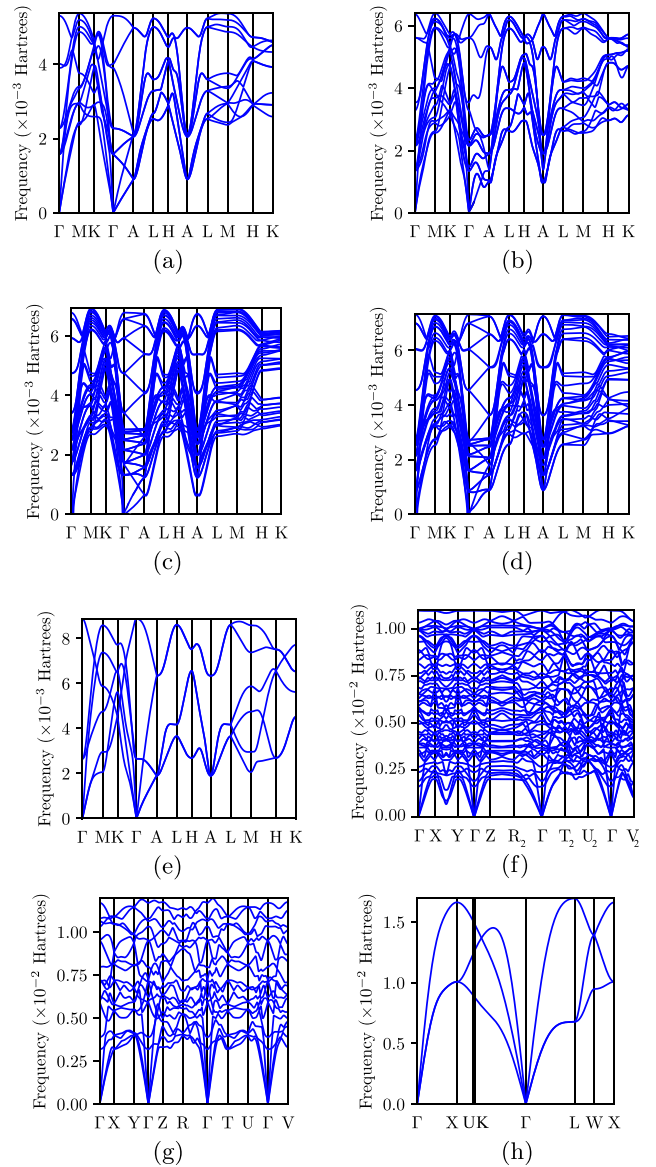
dynamically unstable. We note that whilst most realizations of HG structures in the elements are incommensurate structures, the *Fddd* and *Ibam* phases discussed here are *commensurate* crystals; we show this explicitly for the *Ibam* structure in the Supplemental Material [32].

At 23.6 TPa, we predict a transition from the *Ibam* phase to the fcc structure. As shown in the inset to Fig. 2(b), the fcc phase remains the lowest enthalpy structure over an enormous pressure range; we eventually predict a fcc → bcc transition at 3.93 petapascal (PPa). The dynamical stability of all the structures discussed in this paper is shown in Fig. 6, and structural parameters are shown in Table II.

TABLE II. Structural parameters for the phases discussed in this paper, at selected pressures.

Structure	Pressure (TPa)	Lattice parameters (Å) Wyckoff positions
dhcp	0.80	$a = 2.030$, $c = 6.726$ 2a, 2c
$P6_3/mmc$	1.80	$a = 1.842$, $c = 9.072$ 4f($z = 0.083$), 2b
$P3m1$	1.95	$a = 1.827$, $c = 17.852$ 1a($z = 0$), 1a($z = 0.167$) 1a($z = 0.667$), 1a($z = 0.833$) 1b($z = 0.250$), 1b($z = 0.417$) 1b($z = 0.583$), 1b($z = 0.750$) 1b($z = 0.916$), 1c($z = 0.083$) 1c($z = 0.334$), 1c($z = 0.500$)
$P\bar{6}m2$	2.20	$a = 1.798$, $c = 14.640$ 1d, 1e, 2h($z = 0.100$), 2i($z = 0.200$) 2h($z = 0.300$), 2g($z = 0.400$)
hcp	3.00	$a = 1.726$, $c = 2.787$ 2c
$Fddd$	7.50	$a = 3.771$, $b = 4.083$, $c = 9.681$ 32h($x = 0.000$, $y = 0.000$, $z = 0.361$) 32h($x = 0.000$, $y = 0.321$, $z = 0.000$)
$Ibam$	9.00	$a = 2.545$, $b = 3.547$, $c = 2.881$ 8j($x = 0.406$, $y = 0.167$), 4a
fcc	25.0	$a = 1.778$ 4b

The nature of bonding and the shape of the electronic charge distribution in solids under extreme compression is a topic of interest. The general trend observed is that, with sufficient pressure, all elements tend to eventually form "electride" phases in which electronic charge is localized in interstitial regions between atoms [46]. These interstitial accumulations of electronic charge act as an anionic sublattice, leaving behind a positive charge on the atomic sites; the resulting system, despite being composed of only a single type of element, then behaves like an ionic solid. Figure 7 shows the charge density distributions for the fcc, $Ibam$, $Fddd$, and bcc structures. We find that K does eventually become an electride, but this does not occur until exceptionally high pressures are attained (around 500 TPa). The electride formation pressure in K can be contrasted with the cases of carbon [47], sulfur [28], and aluminium [41], which form terapascal-electrides at pressures of 20 TPa, 1.25 TPa, and 3.2 TPa respectively (all over an order of magnitude lower in pressure than K). In the fcc phase at 3.5 PPa [Fig. 7(a), right], and the bcc phase at 5.0 PPa, [Fig. 7(d)], clear accumulations of interstitial charge can be seen. However, perhaps the most intriguing charge densities are those of the $Fddd$ and $Ibam$ phases; as Figs. 7(c) and 7(b) show, both structures feature "*quasi*-molecules", where some atoms form strongly bonded atomic pairs. In the $Ibam$ phase
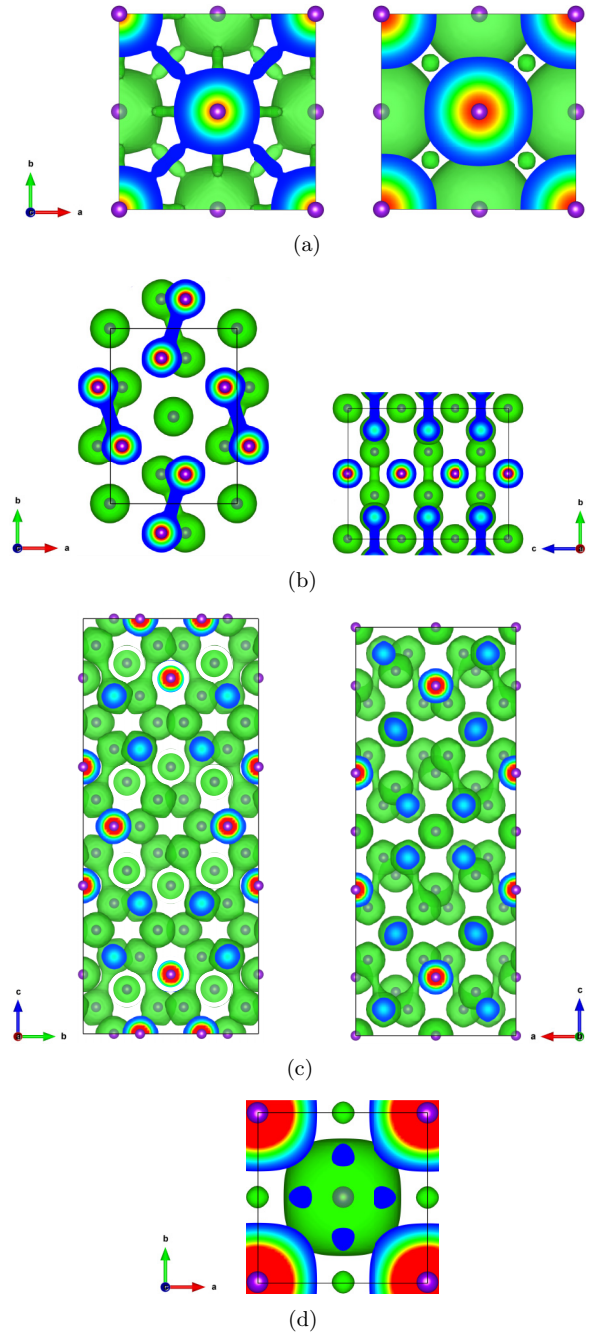

FIG. 7. Charge density isosurfaces at 90% of the valence charge maximum (green) and 2D slices (red/green/blue). K atoms are shown in purple. (a) fcc at 30 TPa (left) and 3.5 PPa (3500 TPa) (right). (b) $Ibam$ at 10 TPa. (c) $Fddd$ at 7.50 TPa. (d) bcc at 5 PPa (5000 TPa).

for example, integrating over these "molecular bonds" using a Bader analysis [48] shows that around 1.3 e of electronic charge is shared between each pair of K atoms; the remaining valence charge is used to form a number of weaker bonds with the remaining atoms. We note that despite the *quasi*-molecular character of the $Fddd$ and $Ibam$ phases, and the significant accumulation of interstitial charge in the electride phases, K remains metallic throughout the entire phase transition sequence.

We have further investigated the electron-phonon coupling properties of elemental K at terapascal pressures. Many elements exhibit record superconducting critical temperatures under compression [38,44], and the question of whether such elements remain superconducting into the TPa range has been raised in several previous publications [28,49]. Superconductivity in K has previously been investigated at much lower pressures [50,51]. We performed electron-phonon coupling calculations within Migdal-Eliashberg theory using density functional perturbation theory (DFPT) in the `QUANTUM ESPRESSO` code [52]. We used the McMillan-Allen-Dynes formula [53] to calculate T_c,

$$T_c = \frac{\omega_{\log}}{1.2} \exp\left(\frac{-1.04(1+\lambda)}{\lambda - \mu^*(1 + 0.62\lambda)}\right). \tag{1}$$

Where $\omega_{\log}$ is the logarithmically averaged phonon frequency, λ is the electron-phonon coupling constant, and μ^* is the Coulomb pseudopotential parameter. Calculations of T_c, especially in elements where T_c is usually of order 10 K or less, require careful treatment and convergence of electron-phonon properties; details regarding our calculations can be found in the Supplemental Material [32].

Figure 8 shows the Fermi-level electronic density of states (eDOS), electron-phonon coupling constant λ and superconducting critical temperature T_c of elemental K for the phases discussed in this paper. We find that the dhcp phase is superconducting with a T_c of 0.75 – 3.87 K, with a rise in T_c upon transition to the $P6_3/mmc$ phase to 2.47 – 7.50 K. Throughout the transition sequence $P6_3/mmc \rightarrow P3m1 \rightarrow P\bar{6}m2$, T_c continues to rise steadily, up to 3.05 – 8.74 K in the $P\bar{6}m2$ phase at 2.30 TPa. A further large increase in T_c occurs upon transition to the hcp phase, with T_c peaking between 7.65 – 15.70 K at around 6.0 TPa. Upon transition to the $Fddd$ and $Ibam$ phases however, there is a dramatic drop in T_c, with T_c falling by over an order of magnitude to just 0.62 – 3.36 K in the $Ibam$ phase at 10.0 TPa. After the $Ibam \rightarrow$ fcc transition at 23.6 TPa, we find that T_c is essentially zero within the precision of our calculations. This dramatic suppression of superconductivity is coincident with a significant reduction in the electron-phonon coupling, which is more than halved in the fcc phase compared to its peak value in the hcp phase. We note however that the eDOS at ϵ_F increases nearly monotonically over the entire transition sequence (see Fig. 8); whilst the number of available states at the Fermi level are increased, their *coupling* to the phonons is reduced. This behavior is qualitatively identical to that of elemental S in the TPa regime [28], which exhibits a large and sudden drop in T_c with sufficient compression.

IV. CONCLUSIONS

We have performed an extensive structure search in elemental K in the terapascal regime, uncovering eight phase transitions beyond the already known dhcp structure, and have incorporated vibrational effects in our calculations to fully elucidate the temperature dependence of the phase boundaries. Our results reveal that under extreme conditions, K adopts the transition sequence dhcp $\rightarrow$ $P6_3/mmc \rightarrow P3m1 \rightarrow P\bar{6}m2 \rightarrow$ hcp $\rightarrow Fddd \rightarrow Ibam \rightarrow$ fcc $\rightarrow$ bcc. The $P6_3/mmc$, $P3m1$, and $P\bar{6}m2$ phases represent
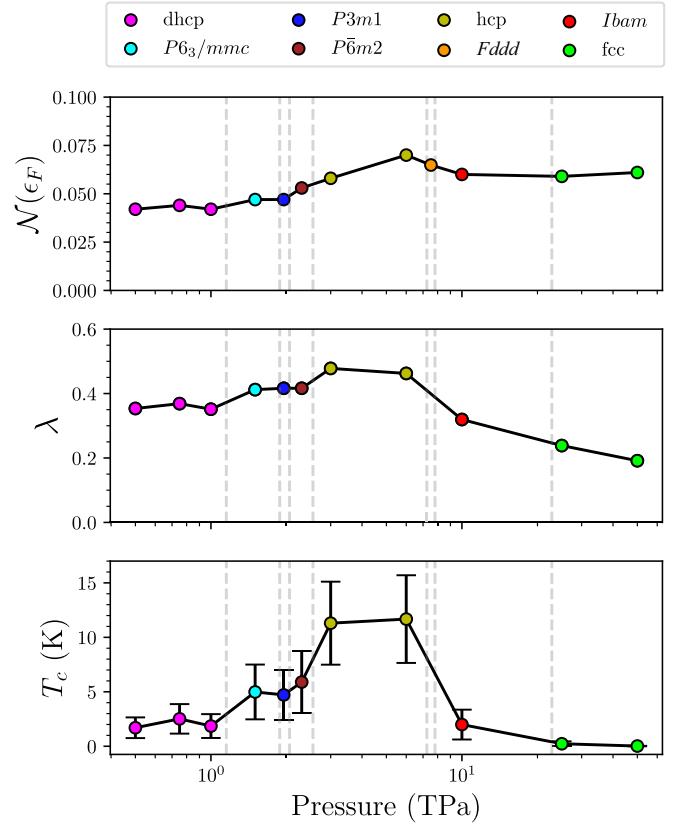

FIG. 8. Electronic properties of the phases: Fermi-level density of states (eDOS) in units of electrons per eV per Å^3, electron-phonon coupling constant λ, superconducting critical temperature T_c. The width of the T_c bars represent values of the Coulomb pseudopotential parameter $\mu^* \in [0.08, 0.12]$. The grey-vertical dotted lines denote the structural phase transitions discussed in this paper. For reasons of computational expense, electron-phonon properties were not computed for the $Fddd$ phase.

particular hexagonal stacking sequences on a pathway between the simpler dhcp and hcp structures, and are only slightly lower in enthalpy than a number of structures from a very large, enthalpically-degenerate manifold of hexagonal motifs in structure space. The complex $Fddd$ and $Ibam$ phases are unlike any other in the sequence, and feature intriguing quasi-molecular bonds between pairs of K atoms. We find that under sufficient compression, K eventually becomes an electride, albeit requiring pressures over an order of magnitude greater than other elements (C, S, and Al) that exhibit electride phases. We have further investigated the electron-phonon coupling properties of K at terapascal pressures, finding that the superconducting T_c peaks between 7.65 – 15.70 K at around 6.0 TPa in the hcp phase, before eventually falling to essentially zero in the fcc phase owing to a significant reduction in electron-phonon coupling.

[1] G. Woolman, V. Naden Robinson, M. Marqués, I. Loa, G. J. Ackland, and A. Hermann, Phys. Rev. Mater. **2**, 053604 (2018).

[2] M. I. McMahon, R. J. Nelmes, U. Schwarz, and K. Syassen, Phys. Rev. B **74**, 140102(R) (2006).

[3] M. Gatti, I. V. Tokatly, and A. Rubio, Phys. Rev. Lett. **104**, 216404 (2010).

[4] Y. Ma, M. Eremets, A. R. Oganov, Y. Xie, I. Trojan, S. Medvedev, A. O. Lyakhov, M. Valle, and V. Prakapenka, Nature (London) **458**, 182 (2009).

[5] Z. Yu, H. Y. Geng, Y. Sun, and Y. Chen, Sci. Rep. **8**, 3868 (2018).

[6] M. Winzenick, V. Vijayakumar, and W. B. Holzapfel, Phys. Rev. B **50**, 12381 (1994).

[7] L. F. Lundegaard, M. Marqués, G. Stinton, G. J. Ackland, R. J. Nelmes, and M. I. McMahon, Phys. Rev. B **80**, 020101(R) (2009).

[8] Y. Ma, A. R. Oganov, and Y. Xie, Phys. Rev. B **78**, 014102 (2008).

[9] R. F. Smith, J. H. Eggert, R. Jeanloz, T. S. Duffy, D. G. Braun, J. R. Patterson, R. E. Rudd, J. Biener, A. E. Lazicki, A. V. Hamza *et al.*, Nature (London) **511**, 330 (2014).

[10] A. Lazicki, D. McGonegle, J. R. Rygg, D. G. Braun, D. C. Swift, M. G. Gorman, R. F. Smith, P. G. Heighway, A. Higginbotham, M. J. Suggit *et al.*, Nature (London) **589**, 532 (2021).

[11] D. E. Fratanduono, M. Millot, D. G. Braun, S. J. Ali, A. Fernandez-Pañella, C. T. Seagle, J.-P. Davis, J. L. Brown, Y. Akahama, R. G. Kraus *et al.*, Science **372**, 1063 (2021).

[12] D. E. Fratanduono, R. F. Smith, S. J. Ali, D. G. Braun, A. Fernandez-Pañella, S. Zhang, R. G. Kraus, F. Coppari, J. M. McNaney, M. C. Marshall, L. E. Kirch, D. C. Swift, M. Millot, J. K. Wicks, and J. H. Eggert, Phys. Rev. Lett. **124**, 015701 (2020).

[13] A. Lazicki, J. R. Rygg, F. Coppari, R. Smith, D. Fratanduono, R. G. Kraus, G. W. Collins, R. Briggs, D. G. Braun, D. C. Swift, and J. H. Eggert, Phys. Rev. Lett. **115**, 075502 (2015).

[14] J. Wang, F. Coppari, R. F. Smith, J. H. Eggert, A. E. Lazicki, D. E. Fratanduono, J. R. Rygg, T. R. Boehly, G. W. Collins, and T. S. Duffy, Phys. Rev. B **94**, 104102 (2016).

[15] S. K. Han, R. F. Smith, D. Kim, J. K. Wicks, J. R. Rygg, A. Lazicki, J. H. Eggert, and T. S. Duffy, Phys. Rev. B **103**, 184109 (2021).

[16] B. J. Henderson, M. C. Marshall, T. R. Boehly, R. Paul, C. A. McCoy, S. X. Hu, D. N. Polsin, L. E. Crandall, M. F. Huff, D. A. Chin, J. J. Ruby, X. Gong, D. E. Fratanduono, J. H. Eggert, J. R. Rygg, and G. W. Collins, Phys. Rev. B **103**, 094115 (2021).

[17] R. Jeanloz, P. M. Celliers, G. W. Collins, J. H. Eggert, K. K. M. Lee, R. S. McWilliams, S. Brygoo, and P. Loubeyre, Proc. Natl. Acad. Sci. USA **104**, 9172 (2007).

[18] M. Millot, S. Zhang, D. E. Fratanduono, F. Coppari, S. Hamel, B. Militzer, D. Simonova, S. Shcheka, N. Dubrovinskaia, L. Dubrovinsky, and J. H. Eggert, Geophys. Res. Lett. **47**, e2019GL085476 (2020).

[19] L. E. Hansen, D. E. Fratanduono, S. Zhang, D. G. Hicks, T. Suer, Z. K. Sprowal, M. F. Huff, X. Gong, B. J. Henderson, D. N. Polsin, M. Zaghoo, S. X. Hu, G. W. Collins, and J. R. Rygg, Phys. Rev. B **104**, 014106 (2021).

[20] D. E. Fratanduono, T. R. Boehly, M. A. Barrios, D. D. Meyerhofer, J. H. Eggert, R. F. Smith, D. G. Hicks, P. M. Celliers, D. G. Braun, and G. W. Collins, J. Appl. Phys. **109**, 123521 (2011).

[21] R. F. Smith, D. E. Fratanduono, D. G. Braun, T. S. Duffy, J. K. Wicks, P. M. Celliers, S. J. Ali, A. Fernandez-Pañella, R. G. Kraus, D. C. Swift *et al.*, Nat. Astron. **2**, 452 (2018).

[22] J. R. Rygg, J. H. Eggert, A. E. Lazicki, F. Coppari, J. A. Hawreliak, D. G. Hicks, R. F. Smith, C. M. Sorce, T. M. Uphaus, B. Yaakobi, and G. W. Collins, Rev. Sci. Instrum. **83**, 113904 (2012).

[23] J. R. Rygg, R. F. Smith, A. E. Lazicki, D. G. Braun, D. E. Fratanduono, R. G. Kraus, J. M. McNaney, D. C. Swift, C. E. Wehrenberg, F. Coppari *et al.*, Rev. Sci. Instrum. **91**, 043902 (2020).

[24] F. Coppari, R. F. Smith, J. Wang, M. Millot, D. Kim, J. R. Rygg, S. Hamel, J. H. Eggert, and T. S. Duffy, Nat. Geosci. **14**, 121 (2021).

[25] Y. Li, Y. Wang, C. J. Pickard, R. J. Needs, Y. Wang, and Y. Ma, Phys. Rev. Lett. **114**, 125501 (2015).

[26] B. Monserrat, N. D. Drummond, C. J. Pickard, and R. J. Needs, Phys. Rev. Lett. **112**, 055504 (2014).

[27] C. J. Pickard, M. Martinez-Canales, and R. J. Needs, Phys. Rev. Lett. **110**, 245701 (2013).

[28] J. Whaley-Baldwin and C. J. Pickard, Phys. Rev. B **105**, 144105 (2022).

[29] C. J. Pickard and R. J. Needs, Phys. Rev. Lett. **97**, 045504 (2006).

[30] C. J. Pickard and R. J. Needs, J. Phys.: Condens. Matter **23**, 053201 (2011).

[31] S. J. Clark, M. D. Segall, C. J. Pickard, P. J. Hasnip, M. I. J. Probert, K. Refson, and M. C. Payne, Z. Kristallogr. - Cryst. Mater. **220**, 567 (2005).

[32] See Supplemental Material at http://link.aps.org/supplemental/10.1103/PhysRevB.107.024106 for pseudopotential information, convergence calculations, details of finite-temperature calculations, details of neural-network fitting and molecular dynamics calculations, evaluation of Lindemann melting criteria, details of electron-phonon calculations and structural information, which includes Refs. [7,34–36,38,41,54].

[33] J. P. Perdew, K. Burke, and M. Ernzerhof, Phys. Rev. Lett. **77**, 3865 (1996).

[34] J. Behler and M. Parrinello, Phys. Rev. Lett. **98**, 146401 (2007).

[35] A. Singraber, mpbircher, S. Reeve, D. W. Swenson, J. Lauret, and philippedavid (2021), CompPhysVienna/n2p2: Version 2.1.4 (v2.1.4), Zenodo, https://doi.org/10.5281/zenodo.4750573.

[36] L. McInnes, J. Healy, and J. Melville, arXiv:1802.03426.

[37] H. Lu, R. Qiu, L. Huang, and T. Tang, Phys. Lett. A **379**, 2479 (2015).

[38] J. Whaley-Baldwin, M. Hutcheon, and C. J. Pickard, Phys. Rev. B **103**, 214111 (2021).

[39] J. Peters and B. Krebs, Acta Crystallogr. Sect. B **38**, 1270 (1982).

[40] B. D. Malone and M. L. Cohen, Phys. Rev. B **85**, 024116 (2012).

[41] C. J. Pickard and R. J. Needs, Nat. Mater. **9**, 624 (2010).

[42] R. J. Nelmes, D. R. Allan, M. I. McMahon, and S. A. Belmonte, Phys. Rev. Lett. **83**, 4081 (1999).

[43] P. Brown, K. Semeniuk, D. Wang, B. Monserrat, C. J. Pickard, and F. M. Grosche, Sci. Adv. **4**, eaao4793 (2018).

[44] S. Arapan, H.-k. Mao, and R. Ahuja, Proc. Natl. Acad. Sci. USA **105**, 20627 (2008).

[45] P. Tsuppayakorn-aek, W. Luo, W. Pungtrakoon, K. Chuenkingkeaw, T. Kaewmaraya, R. Ahuja, and T. Bovornratanaraks, J. Appl. Phys. **124**, 225901 (2018).

[46] M.-S. Miao and R. Hoffmann, Acc. Chem. Res. **47**, 1311 (2014).

[47] M. Martinez-Canales, C. J. Pickard, and R. J. Needs, Phys. Rev. Lett. **108**, 045704 (2012).

[48] W. Tang, E. Sanville, and G. Henkelman, J. Phys.: Condens. Matter **21**, 084204 (2009).

[49] J. Sun, M. Martinez-Canales, D. D. Klug, C. J. Pickard, and R. J. Needs, Phys. Rev. Lett. **108**, 045503 (2012).

[50] G. Profeta, C. Franchini, N. N. Lathiotakis, A. Floris, A. Sanna, M. A. L. Marques, M. Lüders, S. Massidda, E. K. U. Gross, and A. Continenza, Phys. Rev. Lett. **96**, 047003 (2006).

[51] A. Sanna, C. Franchini, A. Floris, G. Profeta, N. N. Lathiotakis, M. Lüders, M. A. L. Marques, E. K. U. Gross, A. Continenza, and S. Massidda, Phys. Rev. B **73**, 144512 (2006).

[52] P. Giannozzi, S. Baroni, N. Bonini, M. Calandra, R. Car, C. Cavazzoni, D. Ceresoli, G. L. Chiarotti, M. Cococcioni, I. Dabo *et al.*, J. Phys.: Condens. Matter **21**, 395502 (2009).

[53] P. B. Allen and R. C. Dynes, Phys. Rev. B **12**, 905 (1975).

[54] M. M. Vopson, N. Rogers, and I. Hepburn, Solid State Commun. **318**, 113977 (2020).